ChemPubSoc Europe

DOI: 10.1002/ejic.201901207

EurJIC European Journal of Inorganic Chemistry

Full Paper

Titanium Carbene Complexes

# *N*-Heterocyclic Carbene and Cyclic (Alkyl)(amino)carbene Complexes of Titanium(IV) and Titanium(III)

Günther Horrer,[a] Mirjam J. Krahfuß,[a] Katharina Lubitz,[a] Ivo Krummenacher,[a,b] Holger Braunschweig,[a,b] and Udo Radius*[a]

**Abstract:** The reaction of one and two equivalents of the *N*-heterocyclic carbene IMes [IMes = 1,3-bis(2,4,6-trimethyl-phenyl)-imidazolin-2-ylidene] or the cyclic (alkyl)(amino)carbene cAAC$^{Me}$ [cAAC$^{Me}$ = 1-(2,6-diisopropyl-phenyl)-3,3,5,5-tetra-methylpyrrolidin-2-ylidene] with [$TiCl_4$] in *n*-hexane results in the formation of mono- and bis-carbene complexes [$TiCl_4$(IMes)] **1**, [$TiCl_4$-(IMes)$_2$] **2**, [$TiCl_4$(cAAC$^{Me}$)] **3**, and [$TiCl_4$(cAAC$^{Me}$)$_2$] **4**, respectively. For comparison, the titanium(IV) NHC complex [$TiCl_4$(I*i*Pr$^{Me}$)] **5** (I*i*Pr$^{Me}$ = 1,3-diisopropyl-4,5-dimethyl-imidazolin-2-ylidene) has been synthesized and structurally characterized. The reaction of [$TiCl_4$(IMes)] **1** with $PMe_3$ affords the mixed substituted complex [$TiCl_4$(IMes)($PMe_3$)] **6**. The reactions of [$TiCl_3$(THF)$_3$] with two equivalents of the carbenes IMes and cAAC$^{Me}$ in *n*-hexane lead to the clean formation of the titanium(III) complexes [$TiCl_3$(IMes)$_2$] **7** and [$TiCl_3$(cAAC$^{Me}$)$_2$] **8**. Compounds **1**–**8** have been completely characterized by elemental analysis, IR and multinuclear NMR spectroscopy and for **2**–**5**, **7** and **8** by X-ray diffraction. Magnetometry in solution, EPR and UV/Vis spectroscopy and DFT calculations performed on **7** and **8** are indicative of a predominantly metal-centered $d^1$-radical in both cases.

## Introduction

Since the first synthesis and isolation of *N*-heterocyclic carbenes (NHCs),[1] these carbenes and related molecules such as cyclic (alkyl)(amino)carbenes (cAACs)[2,3] have not only become a considerable alternative to phosphines as ancillary ligands in transition metal chemistry, especially in homogeneous catalysis,[4] but they also have found versatile applications on their own, for example in organocatalysis.[5] The particular stereo-electronic properties, i.e. the combination of the characteristic strong σ-donor properties along with the easily adjustable steric demand enables the stabilization of many low-valent metals in various oxidation states and different coordination spheres, mainly for the more electron rich transition metals in low to middle oxidation states.

More recently, the chemistry of high-oxidation state 3d metals featuring NHC and cAAC ligands gained increasing interest.[6] However, as one of the interesting properties of NHC and cAAC complexes of late transition metals is their robustness and stability, the (thermal) stability of complexes with early transition metals seems to be an intrinsic issue. Calculations performed on various transition metal NHC complexes reveal that the bonding situation between NHCs and high oxidation state early transition metals becomes quite different as compared to the interaction with electron rich transition metals in low to middle oxidation states.[7] To assess the M–C orbital interaction in transition metal NHC complexes completely, three interactions are of relevance (see Scheme 1, i): (top) the σ-donation from the occupied NHC σ-donor orbital to a transition metal acceptor orbital, (middle)

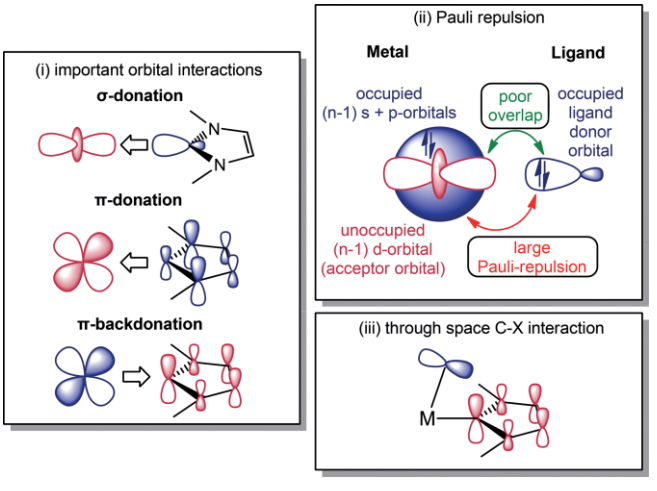


Scheme 1. (i) Important orbital interactions between a NHC ligand and an electron-poor high-oxidation-state 3d metal ion: σ-donation, π-donation and π-backdonation; (ii) a schematic illustration of the Pauli repulsion between the ligand donor orbital and the occupied outermost core (*n*–1)s and (*n*–1)p shells in a transition metal complex, leading to poor overlap between the transition metal (*n*–1)d acceptor orbital and the NHC ligand σ-donor orbital; (iii) schematic illustration of the X-ligand p-orbital interaction with the carbene $p_\pi$-orbital in high-oxidation-state transition metal carbene complexes.

[a] *Institut für Anorganische Chemie, Julius-Maximilians-Universität Würzburg, Am Hubland, 97074 Würzburg, Germany*
*E-mail: u.radius@uni-wuerzburg.de*
*http://www.ak-radius.de*
[b] *Institute for Sustainable Chemistry & Catalysis with Boron, Julius-Maximilians-Universität Würzburg, Am Hubland, 97074 Würzburg, Germany*

*Supporting information and ORCID(s) from the author(s) for this article are available on the WWW under https://doi.org/10.1002/ejic.201901207.*

delocalization of the occupied NHC π-system into an unoccupied transition metal $d_\pi$-orbital, i.e. π-donation, and (bottom) π-backdonation from an occupied transition metal $d_\pi$-orbital into the NHC carbon $p_\pi$-orbital.

NHCs and cAACs are strongly σ-donating in nature, and the HOMO of these carbon-based ligands are more diffuse and much higher in energy compared to those of nitrogen- and oxygen-based ligands typically employed in the stabilization of early transition metals. This can result in a more effective orbital overlap between the NHC HOMO and the 3d-orbitals of metal ions, but also in a much more ionic metal carbon interaction compared to late transition metals due to the large energy gap between the HOMO of the NHC and the 3d acceptor orbital or – to put it to an extreme – to electron transfer from the ligand to the metal in a redox reaction between the NHC and the high-oxidation-state transition metal species. Furthermore, π-contributions should be small for the interaction with metals in their highest oxidation states, since for π-donation the coefficients of the carbene C($p_\pi$) orbitals are rather small which leads to only small overlap with the corresponding metal d-orbital, whereas π-backdonation should not be possible for $d^0$-metal complexes, but should be of growing importance with increasing d-electron count.

Even if there is a good σ-donor interaction between the NHC and the highest oxidation state 3d metals, it should be much weaker as compared to the interaction with 4d and 5d metals, but also with electron-rich 3d metals. It has been shown that Pauli repulsion between the inner occupied 3s- and 3p-orbitals of 3d metals and donor orbitals of the ligand weakens the M–L bond strengths substantially (see Scheme 1, ii).[8] The 3d-orbitals have no radial nodes, which leads to a limited spatial extension of the metal 3d-orbitals and thus to a similar size of 3s-, 3p-, and 3d-shells of the metal. Interaction of the "small" metal 3d-orbitals with the occupied σ-donating orbital of the ligand leads to short M–L distances with poor M(3d)–L(σ) overlap and thus to a comparable high Pauli repulsion between the occupied σ-donating orbital of the ligand and the inner, occupied 3s- and 3p-orbitals of the transition metal which are close in space (Scheme 1, ii). Both factors result in inefficient 3d metal–ligand interactions, especially for high-oxidation-state metal species, as their 3d-orbitals have more contracted radial distributions.

Only a few theoretical studies on the orbital interaction of M–C(NHC) bonds of early transition metal complexes of metals in their higher or highest oxidation state (electronic configuration $d^0$-$d^2$) are currently available. Jacobsen and co-worker calculated in an EDA study on the $3d^0$ complexes $[TiCl_5(IH)]^-$, $[(\eta^5\text{-}C_5H_5)_2Ti(IH)Me]^+$, and $[V(=O)Cl_3(IH)]$ (IH= Imidazolin-2-ylidene)[7a,7b] by using DFT methods a bond snapping energy of the M–C bonds of approximately 110, 240, and 180 kJ/mol, respectively, and corresponding orbital interaction energies $\Delta E_{orb}$ of ca. –220, –240, and –310 kJ/mol. The latter can be divided into σ-contributions of the orbital interactions of 89 %, 82 %, and 89 %, respectively, and π-contributions of 11 %, 18 %, and 11 %. The data clearly indicate the dominant role of σ-interactions in these metal–NHC bonds. A similar study of the Frenking group on neutral $[TiCl_4(IH)]$ revealed σ- and π-interaction energies of the Ti–C bond to be –214 and –32 kJ/mol, respectively, and that the π-interaction can be divided into ligand-to-metal π-donation and metal-to-ligand π-backbonding interactions of approximately the same magnitude (both –16 kJ/mol).[7b] The latter is quite unusual for a $d^0$ metal without any electron in the d-shell, and population of the NHC carbene carbon $p_\pi$*-orbital was rationalized with charge transfer from either a delocalized Cl–Ti–C(NHC) π-interaction of an occupied chloride $p_\pi$-orbital via an unoccupied titanium d-orbital into the unoccupied NHC carbene carbon $p_\pi$*-orbital, or from the direct charge transfer from a chloride p-orbital of a neighboring chloride ligand into the NHC carbene carbon $p_\pi$*-orbital through space. The latter would be associated with a distortion of the molecule and with relatively short Cl–C(NHC) distances (see Scheme 1, iii). This kind of distortion was observed on several occasions in the X-ray crystal structures of NHC-stabilized transition metal halides in high oxidation states (see also below). Furthermore, this through-space interaction between the NHC carbon atom and the chloride ligand should be also relevant to energetically low-lying decomposition pathways of NHC-stabilized high-valent transition metal complexes, as it is a pre-aggregation on the pathway to the transition state of a reductive elimination step to give imidazolium salts. Note that for the synthesis of many of the NHC complexes of early transition metals known to date tethered ligands are employed with chelating alkoxide, amide, imide etc. moieties as anchoring groups, which lead to a more robust ligand environment for these complexes.

## Results and Discussion

In light of these issues we want to systematically explore the coordination chemistry of NHCs and related ligands in early transition metal complexes, using these neutral carbon donor ligands without any anchoring group. Group 4 NHC complexes, primarily of the higher congeners of titanium, i.e. zirconium and hafnium, already exist. Although there are also a couple of NHC titanium(IV) complexes known, we decided to start our investigations by exploring the reactivity of NHCs and cAACs with respect to titanium(IV) and titanium(III) chlorides. The first NHC-stabilized complexes of titanium(IV), $[TiCl_4(IMe)]$ (IMe = 1,3-dimethyl-imidazolin-2-ylidene) and $[TiCl_4(I\mathit{i}PrMe)]$ **5** (I*i*PrMe = 1,3-diisopropyl-4,5-dimethyl-imidazolin-2-ylidene), have been reported by Herrmann et al. in 1994 and by Kuhn et al. in 1995.[9] The reaction of the free carbenes with $[TiCl_4(THF)_2]$ and $[TiCl_4]$, respectively, led to the formation of these complexes. Unfortunately, no molecular structures of the mono-NHC substituted compounds were obtained and are still hitherto unknown. However, Kuhn et al. were able to obtain the molecular structure of the closely related dinuclear μ-oxo bridged titanium complex $[(I\mathit{i}PrMe)TiCl_3\text{–}O\text{–}TiCl_3(I\mathit{i}PrMe)]$ by careful hydrolysis of $[TiCl_4(I\mathit{i}PrMe)]$ **5**. In the following years, the synthesis of various NHC compounds of zirconium and hafnium were reported until the group around Hahn synthesized the benzannulated mono-NHC titanium complex $[TiCl_4(L)]$ {L = *N*,*N*′-bis(2,2-dimethylpropyl)benzimidazolin-2-ylidene} with the sterically demanding dimethyl propyl substituents in 2004.[10] This complex is in fact also the first molecular structure reported for a mono-NHC titanium(IV) chloride complex with a penta-coordinated titanium center.[10] In the same

year, Cowley et al. demonstrated that the synthesis of mono-NHC titanium complexes like $[TiCl_2(NMe_2)_2IMes]$ is also feasible via amine-elimination of $[Ti(NMe_2)_4]$ using two equivalents of 1,3-dimesityl-imidazolium chloride as the NHC source.[11] This elegant synthetic route also avoids the previous preparation and purification of the corresponding carbene. In 2008, Roesky and co-workers synthesized and structurally characterized two bis-carbene fluoride complexes $[TiF_4(IMe_4)_2]$ ($IMe_4$ = 1,3,4,5-tetramethylimidazolin-2-ylidene) and $[TiF_4(IiPrMe)_2]$ with the carbene ligands located in *trans* positions.[12] Fischer et al. reported in 2013 the synthesis and structural characterization of both, the mono-NHC coordinated complex $[TiCl_4(IDipp)]$ {IDipp = 1,3-bis(2,6-diisopropylphenyl)imidazolin-2-ylidene} and the bis-carbene complexes $[TiCl_4(IDipp)_2]$ and $[TiF_4(IDipp)_2]$.[13] The further reaction of $[TiCl_4(IDipp)]$ with $ZnMe_2$ did not result in the desired methylated titanium complex $[TiMe_4(IDipp)]$, but leads instead to the neutral zinc complex $[ZnCl_2(IDipp)]$. A NHC-stabilized $[TiMe_4]$ complex was never observed or isolated so far.[13] This behavior, i.e. transfer of the NHC from titanium to zinc, may also be considered as an experimental support for the calculated low dissociation energies of the Ti–NHC bonds (vide supra), since the formation of the Zn–NHC bond seems to be clearly preferred over formation of a Ti–NHC bond.

There are far less examples of carbene-stabilized $Ti^{III}$ complexes. A first report of complexes of this type, $[TiCl_2(NMe_2)(IMes)_2]$ and $[TiCl_3(IDipp)_2]$, were presented including X-ray diffraction analyses by Lorber et al. in 2009 and by Roesky et al. in 2010, respectively.[14] Lorber et al. also reported an attempt to synthesize the $[TiCl_3(IMes)_2]$ complex, but they did not succeed to obtain the expected product.[14a]

In the beginning of our work, we aimed at the synthesis and structural characterization of mono- and bis-carbene stabilized $Ti^{IV}$ and $Ti^{III}$ complexes using IMes and $cAAC^{Me}$ as the ligands. We reasoned that the often-employed starting material $[TiCl_4(THF)_2]$ should not be used as a precursor for this type of chemistry, as the bond dissociation energy (BDE) of the Ti–NHC and Ti–$cAAC^{Me}$ bond should be low. DFT calculations have been performed on the BP86//def2-TZVP(Ti)/def2-SV(P)-level of theory to calculate the average BDEs of different complexes of the type $[TiCl_4(L)_2]$ for the dissociation into 2 L and $[TiCl_4]$. As a result (see Table 1), the mean BDE for the complexes $[TiCl_4(NHC)_2]$ and $[TiCl_4(cAAC^{Me})_2]$ is way lower than the BDE values usually calculated for many other NHC transition metal complexes. However, the mean BDE of $[TiCl_4(THF)_2]$ is less compared to the BDEs calculated for the NHC complexes (cf. BDE $[TiCl_4(THF)_2]$ = -33.0 kJ/mol and BDE $[TiCl_4(IiPr)]$ = –92.2 kJ/mol, see Table 1). On the other hand, the mean BDE for the excellent σ-donor/π-acceptor $cAAC^{Me}$ (–47.3 kJ/mol) is much lower compared to the mean BDE calculated for the NHC complexes (–74.8 kJ/mol to –92.2 kJ/mol) and are rather in the range calculated for the THF complex (–33.0 kJ/mol). The latter is in line with the peculiarities of the bonding in these complexes as outlined in the introduction.

Table 1. Average calculated bond dissociation energies in kJ/mol for the dissociation of $[TiCl_4(L)_2]$ into 2 L and $[TiCl_4]$. Calculations have been performed on the BP86//def2-TZVP(Ti)/def2-SV(P)-level of theory.

| L | BDE [kJ/mol] |
|---|---|
| THF | –33.0 |
| IMes | –74.8 |
| $cAAC^{Me}$ | –47.3 |
| I*i*PrMe | –81.9 |
| I*i*Pr | –92.2 |

To avoid the formation of undesired (mixed) THF complexes, we decided to react the corresponding free carbene with freshly distilled $[TiCl_4]$ in *n*-hexane at –78 °C. This simple, yet efficient synthesis leads to $[TiCl_4(IMes)]$ **1** as a pale yellow solid in 74 % yield after workup, and $[TiCl_4(cAAC^{Me})]$ **3** was obtained in 84 % yield as a yellow solid (see Scheme 2). Further reaction with an additional equivalent of the corresponding carbene or the reaction of $[TiCl_4]$ with two equivalents of the carbene resulted in the formation of the bis-carbene complexes $[TiCl_4(IMes)_2]$ **2** and $[TiCl_4(cAAC^{Me})_2]$ **4** as bright yellow and bright red solids, respectively. However, the reaction of $[TiCl_4]$ with two equivalents of the carbenes is sluggish and undesired side products were formed from time to time which were hard to separate. Thus, to our experience it is advantageous to isolate the mono-carbene complexes and react them with an additional equivalent of the carbene. Using this procedure, the bis-carbene complexes $[TiCl_4(IMes)_2]$ **2** and $[TiCl_4(cAAC^{Me})_2]$ **4** were formed in excellent yields of 89 % and 91 %, respectively. This route is also viable for the formation of mixed ligated complexes, as exemplified by the synthesis of $[TiCl_4(IMes)(PMe_3)]$ **6** in 70 % isolated yield from the reaction of **1** with $PMe_3$ in *n*-hexane at –78 °C.

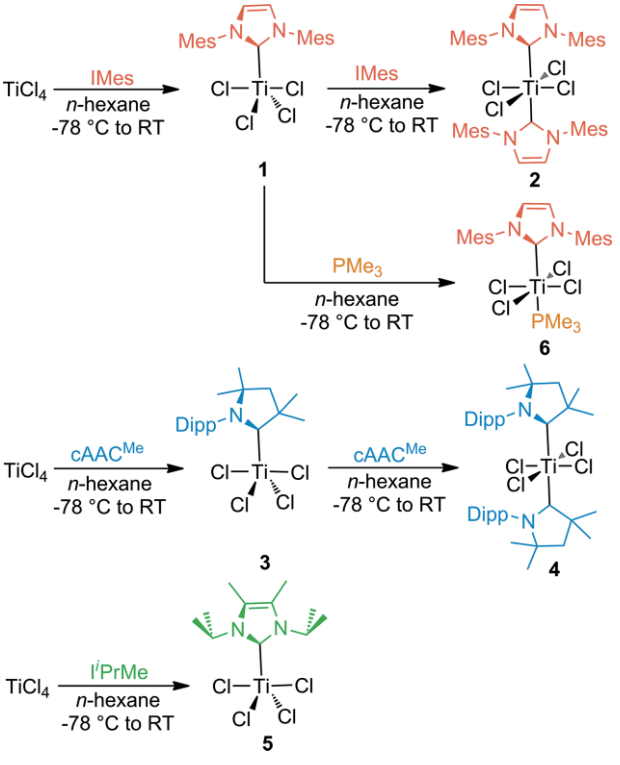


Scheme 2. Synthesis of the titanium(IV) complexes **1**–**6**.

We also synthesized the complex $[TiCl_4(IiPrMe)]$ **5** from the reaction of I*i*PrMe with $[TiCl_4]$ in *n*-hexane. This complex has been reported before by Kuhn et al. in 1995 but was not structur-

ally characterized at that time. [$TiCl_4$(l*i*PrMe)] **5** was obtained as bright red solid in 68 % yield after workup. The NMR spectroscopic data is in perfect agreement with those reported by Kuhn et al. earlier.[9b]

The complexes **1**–**6** are highly moisture and air sensitive solids, which are, with the exception of **1**, well soluble in benzene and toluene and almost insoluble in *n*-hexane. We examined the stability of some of these complexes with respect to ligand exchange of the carbene ligands. The bis-carbene complex [$TiCl_4$(IMes)$_2$] **2** is stable in benzene solution in the presence of weak neutral two electron donors such as THF, as already indicated by the calculations of the BDEs for the titanium(IV) NHC and cAAC$^{Me}$ complexes with respect to [$TiCl_4$(THF)$_2$]. However, [$TiCl_4$(IMes)$_2$] **2** readily decomposes in THF solution and in the presence of the nitrogen containing donor molecules such as acetonitrile or pyridine. In the case of pyridine, trace amounts of decomposition can already be observed at room temperature, but slight heating of the mixture to temperatures of 40 °C and beyond leads to decomposition of the complex with the release of free IMes ligand but without the formation of the pyridine adduct [$TiCl_4$(py)$_2$] (see SI Figure S1b).

The compounds **1**–**6** were fully characterized by means of elemental analysis, IR, $^1$H and $^{13}$C{$^1$H} NMR spectroscopy, which unambiguously confirm the formation of the complexes. The $^1$H and $^{13}$C{$^1$H} NMR spectra of [$TiCl_4$(IMes)] **1**, [$TiCl_4$(IMes)$_2$] **2**, and [$TiCl_4$(IMes)(PMe$_3$)] **6** show one set of signals each for the NHC ligand with resonances which are slightly shifted from each other. The $^1$H NMR spectra reveal two singlets for the methyl-groups of the mesityl-substituent in *para*- and *ortho*-position (**1**: 2.01 ppm and 2.21 ppm; **2**: 2.10 ppm and 2.27 ppm; **6**: 2.13 ppm and 2.34 ppm). The resonances associated with the aryl protons are detected as a singlet at 6.68 ppm (**1**), 6.67 ppm (**2**) and 6.80 ppm (**6**), whereas the NHC backbone protons give rise to resonances at 5.85 ppm (**1**), 5.91 ppm (**2**) and 6.02 ppm (**6**). Similarly, one set of resonances is observed for the IMes ligand in the $^{13}$C{$^1$H} NMR spectra of these compounds, and most significantly the resonances for carbene carbon atoms are observed at 186.4 ppm (**1**), 190.1 ppm (**2**) and 190.4 ppm (**6**), which are at higher field compared to the uncoordinated Arduengo carbene ($\delta$ = 243.8 for IMes). The complex [$TiCl_4$(IMes)(PMe$_3$)] **6** gives rise to a resonance at –8.05 ppm in the $^{31}$P NMR spectrum. Similarly, the $^1$H and $^{13}$C{$^1$H} NMR spectra of the complexes **3** and **4** reveal one set of resonances for the cAAC$^{Me}$ ligands with resonances of the carbene carbon atom at 260.3 ppm (**3**) and 264.2 ppm (**4**) in the $^{13}$C{$^1$H} NMR spectra (see also Table 2). These resonances are also significantly shifted compared to the free cAAC$^{Me}$ ($\delta$ = 304.2 ppm). In case of compound **4**, broadened resonances were detected in the $^1$H NMR which suggests the presence of a equilibrium between the bis-carbene complex **4** and the mono-carbene compound **3** and free cAAC$^{Me}$ in solution (see SI Figure S8 and S9).

The complexes [$TiCl_4$(IMes)$_2$] **2**, [$TiCl_4$(cAAC$^{Me}$)] **3**, [$TiCl_4$-(cAAC$^{Me}$)$_2$] **4** and [$TiCl_4$(l*i*PrMe)] **5** have been structurally characterized. Single-crystals suitable for X-ray diffraction of **2**, **3** and **4** were obtained by vapour diffusion of *n*-hexane into a saturated solution of the compound in benzene at room temperature, high quality crystals of **5** have been obtained by storing a saturated solution of **5** in *n*-hexane over one week at –30 °C (Figure 1).

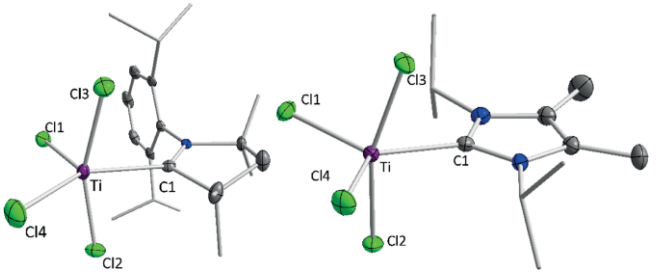


Figure 1. Molecular structures of [$TiCl_4$(cAAC$^{Me}$)] **3** (left) and [$TiCl_4$(l*i*PrMe)] **5** (right) in the solid state. Hydrogen atoms are omitted for clarity. Atomic displacement ellipsoids are set at 50 % probability. Selected bond lengths [Å] and angles [°] for **3**: Ti–C1 2.1976(31), Ti–Cl1 2.1909(10), Ti–Cl2 2.2418(10), Ti–Cl3 2.2840(11), Ti–Cl4 2.2606(11), C1–Cl2/Cl3 2.9230(31)/2.8750(31), C1–Cl1 3.6500(31), C1–Cl4 4.1032(31), C1–Ti–Cl1 112.54(9), C1–Ti–Cl2 82.37(9), C1–Ti–Cl3 79.77(9), C1–Ti–Cl4 133.96(6), Cl1–Ti–Cl2 99.18(4), Cl1–Ti–Cl3 100.11(4), Cl1–Ti–Cl4 113.47(4), Cl2–Ti–Cl3 157.58(4), Cl2–Ti–Cl4 91.77(4), Cl3–Ti–Cl4 90.95(4). Selected bond lengths [Å] and angles [°] for [TiCl4(l*i*PrMe)] **5**: Ti–C1 2.1759(14), Ti–Cl1 2.2103(4), Ti–Cl2 2.2607(4), Ti–Cl3 2.2807(4), Ti–Cl4 2.2218(5), C1–Cl2/Cl3 2.8852(14)/2.8578(14), C1–Cl1 3.8339(14), C1–Ti–Cl1 121.87(4), C1–Ti–Cl2 81.10(4), C1–Ti–Cl3 79.73(4), C1–Ti–Cl4 128.07(4), Cl1–Ti–Cl2 96.662(16), Cl1–Ti–Cl3 96.209(16), Cl1–Ti–Cl4 110.042(18), Cl2–Ti–Cl3 160.555(18), Cl2–Ti–Cl4 95.094(18), Cl3–Ti–Cl4 94.112(17).

The mono-carbene complexes **3** and **5** crystallize in the space group $P2_1/c$ (**3**) and $P2_1/n$ (**5**) with one molecule in the asymmetric unit. Both complexes adopt a distorted trigonal bipyramidal structure (see Figure 1), in which the carbene ligand, Cl1 and Cl4 occupy the equatorial positions while Cl2 and Cl3 lie in the highly distorted axis of the polyhedron. The Ti–C distance of 2.1976(31) Å (**3**) and 2.1759(14) Å (**5**) are similar to those of Ti–$C_{carbene}$ bonds reported earlier, which lie in a range within 2.16 and 2.35 Å for both mono- and bis-carbene complexes of titanium.[6b]

Notably, the Ti–C distance in **5** [2.1759(14) Å] is significantly shorter than the Ti–C distance observed for the cAAC$^{Me}$ substituted complex **3** [2.1909(10) Å], presumably due to stronger Pauli

Table 2. $^{13}$C{$^1$H} and $^{31}$P NMR resonances of the ligating atoms as well as the yields of the synthesis for the complexes [$TiCl_4$(IMes)] **1**, [$TiCl_4$(IMes)$_2$] **2**, [$TiCl_4$(cAAC$^{Me}$)] **3**, [$TiCl_4$(cAAC$^{Me}$)$_2$] **4**, [$TiCl_4$(l*i*PrMe)$_2$] **5** and [$TiCl_4$(IMes)(PMe$_3$)] **6**.

| Compound | $\delta$ = $^{13}C_{Carbene}$ [ppm] | $\delta$ = $^{31}$P [ppm] | yield [%] |
|---|---|---|---|
| [$TiCl_4$(IMes)] **1** | 186.4 | – | 74 |
| [$TiCl_4$(IMes)$_2$] **2** | 190.1 | – | 84 |
| [$TiCl_4$(cAAC$^{Me}$)] **3** | 260.3 | – | 89 |
| [$TiCl_4$(cAAC$^{Me}$)$_2$] **4** | 264.2 | – | 91 |
| [$TiCl_4$(l*i*PrMe)] **5** | 185.3 | – | 68 |
| [$TiCl_4$(IMes)(PMe$_3$)] **6** | 190.4 | –8.04 | 71 |

repulsion in complex **3**. The axial chloride ligands Cl2 and Cl3 of **3** are bent towards the carbene carbon atom with an angle Cl2–Ti–Cl3 of 157.58(4), one reason for this bending might be a through space C–X interaction as shown in Scheme 1, iii. The angle Cl2–Ti–Cl3 observed in **5** of 160.555(18)° is larger than that of **3.** Furthermore, the axis in **3** is asymmetrically distorted with angles of 79.77(9)° (C1–Ti–Cl3) and 82.37(9)° (C1–Ti–Cl2), which leads to relatively short C1–Cl2/Cl3 distances of 2.9230(31) Å and 2.8750(31) Å. Both distances are within the sum of the van-der-Waals-radii of carbon and chlorine atoms (3.45 Å) and confirm some intramolecular ligand-ligand interaction, for example interaction between the empty carbene $p_z$-orbital with the lone pairs of the chloride ligands, which has already been observed for similar titanium(IV) complexes and discussed above (see Scheme 1).[6c,11,14b,15]

The bis-carbene complexes **2** and **4** crystallize in the triclinic space group $P\bar{1}$ with one additional solvent molecule benzene (**2**) or *n*-hexane (**4**) in the asymmetric unit. Both complexes adopt a distorted octahedral structure, in which the carbene ligands are located in *trans*-position to each other (Figure 2). The chloride ligands are mutually pairwise (Cl1/Cl2 and Cl3/Cl4) distorted toward the carbene ligands. The Ti–C1/C2 bond lengths of 2.3309(55) Å and 2.3294(55) Å of $[TiCl_4(cAAC^{Me})_2]$ **4** are slightly elongated in comparison to the Ti–C1 bond length in the mono-$cAAC^{Me}$ complex **3** (see Table 3). The carbene ligands are twisted to each other with an angle between the best planes through the five-membered carbene core of 74.69(16)° for **2** and 68.73(57)° for **4** to each other.

As a result of this twisting, an intra-ligand interaction between the carbene carbon $p_\pi$-orbitals and the lone pairs at the chloride ligands Cl1/Cl2 and Cl3/Cl4 would be possible. However, this deviations from the ideal bond angles of octahedral $d^0$ complexes of the type $[TiCl_4(NHC)_2]$ and $[TiCl_4(cAAC^{Me})_2]$ can also be attributed to a second-order Jahn–Teller distortion of the ideal octahedron (see Figure 3).[16] The reduction of the octahedral symmetry of the complex leads to a mixing of the occupied $1t_{1u}$-orbitals of the octahedral complex, which are a linear combination of ligand σ-type orbitals and titanium 4p-orbitals and are the highest occupied σ-bonding orbitals of the complexes, with the low lying, unoccupied $1t_{2g}$ set of orbitals, which are all titanium 3d in character. This admixture of titanium 3d into $1t_{1u}$ results in the formation of an occupied, energetically stabilized and thus lower-lying $\varphi_1$-hybrid orbital, which has better overlap to the ligand orbitals and makes thus a stronger σ-bond to the ligand. In addition, an unoccupied, virtual $\varphi_2$-orbital is formed. Such second-order Jahn–Teller distortions are typical for octahedral $ML_6$ complexes with low electron count, and similar observations have also been made for related zirconium complexes $[ZrCl_4(NHC)_2]$.[17] Presumably both effects, the second order Jahn–Teller distortion to strengthen M–L bonding as well as an interaction of the lone pairs of the chloride ligands with the unoccupied carbene $p_z$-orbital, contribute to the stability of the complex.

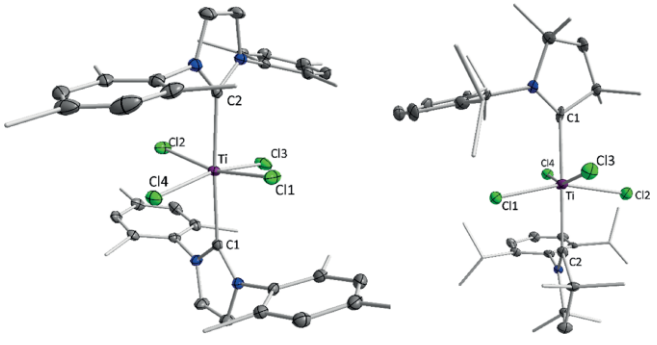


Figure 2. Molecular structures of $[TiCl_4(IMes)_2]$ **2** (left) and $[TiCl_4(cAAC^{Me})_2]$ **4** (right) in the solid state. Hydrogen atoms and a co-crystallized molecule of benzene/*n*-hexane in case of **2**/**4** are omitted for clarity. Atomic displacement ellipsoids are set at 50 % probability. Selected bond lengths [Å] and angles [°] for **2**: Ti–C1/C2 2.3358(15)/2.3343(14), C1–Cl3/Cl4 3.0619(13)/3.0619(13), C2–Cl1/Cl2 3.0153(17)/3.0835(16), C1–Ti–C2 175.95(5), Cl1–Ti–Cl2 165.09(2), Cl3–Ti–Cl4 166.11(2), C1–Ti–Cl3/Cl4 83.07(4)/83.30(4), C2–Ti–Cl1/Cl2 81.62(4)/83.65(4). Relevant bond lengths [Å] and angles [°] for **4**: Ti–C1/C2 2.3309(55)/2.3294(55), C1–Cl3/Cl4 2.8522(48)/3.1288(50), C2–Cl1/Cl2 2.9954(56)/3.0078(56), C1–Ti–C2 177.62(18), Cl1–Ti–Cl2 160.59(6), Cl3–Ti–Cl4 160.18(6), C1–Ti–Cl3 75.17(12)/85.97(13), C2–Ti–Cl1/Cl2 80.93(13)/80.42(13).

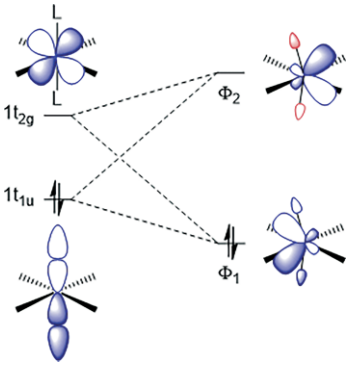


Figure 3. Schematic representation of the second-order Jahn–Teller distortion in octahedral complexes $d^0$-$ML_6$: orbital mixing of $t_{1u}$- and $t_{2g}$-type orbitals (denoted according to $O_h$ symmetry) leads to the formation of one occupied, energetically lower-lying, $\varphi_1$-hybrid orbital and one unoccupied $\varphi_2$-orbital.

Carbene-stabilized titanium(III) complexes can be obtained starting from $[TiCl_3(THF)_3]$. However, Lorber et al. reported before that the reaction of $[TiCl_3(THF)_3]$ with 2 equiv. of IMes in THF

Table 3. Important bond lengths and distances of the complexes **1**–**8** (*: distances to the nearest chloride ligand).

| Compound | Ti–C1/C2 [Å] | C1–Cl* [Å] |
|---|---|---|
| $[TiCl_4(IMes)]$ **1** | – | – |
| $[TiCl_4(IMes)_2]$ **2** | 2.3358(15) / 2.3343(14) | 3.0619(13) / 3.0619(13) |
| $[TiCl_4(cAAC^{Me})]$ **3** | 2.1976(31) | 2.8750(31) / 2.9230(31) |
| $[TiCl_4(cAAC^{Me})_2]$ **4** | 2.3309(55) / 2.3294(55) | 2.8522(48) / 3.1288(50) |
| $[TiCl_4(I\!i\!PrMe)]$ **5** | 2.1759(14) | 2.8578(14) / 2.8852(14) |
| $[TiCl_4(IMes)(PMe_3)]$ **6** | – | – |
| $[TiCl_3(IMes)_2]$ **7** | 2.3268(40) / 2.3379(37) | – |
| $[TiCl_3(cAAC^{Me})_2]$ **8** | 2.2991(12) / 2.2793(42) | – |

did not afford the expected complex $[TiCl_3(IMes)_2]$, but produced instead an insoluble material that was characterized on the basis of combustion analysis as $[TiCl_3(IMes)(THF)_2]$.[14a] We have found now that the choice of solvent is also crucial here. The treatment of a suspension of $[TiCl_3(THF)_3]$ in *n*-hexane with two equivalents of IMes or $cAAC^{Me}$ at –78 °C leads to the formation of blue $[TiCl_3(IMes)_2]$ **7** and violet $[TiCl_3(cAAC^{Me})_2]$ **8** (see Scheme 3).

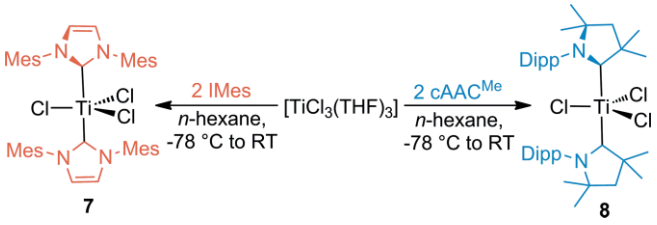


Scheme 3. Synthesis of **7** and **8**.

The starting material $[TiCl_3(THF)_3]$ is, compared to $cAAC^{Me}$ and IMes, hardly soluble in *n*-hexane, but its solubility is good enough to lead to the desired product in good yield. Both compounds were characterized by elemental analysis, magnetometry in solution, IR, EPR and UV/Vis spectroscopy. Using the Evans method, the magnetic moment of **7** in solution was determined to $\mu$ = 1.74 $\mu_B$, which is in good agreement with an expected $\mu_B$ between 1.6 – 1.8 for $d^1$-titanium complexes. For **8**, a magnetic moment of $\mu$ = 2.47 $\mu_B$ was observed, which lies above the expected spin-only value of 1.73 $\mu_B$ and below a spin only value for two unpaired electrons (i.e. $\mu$ = 2.83 $\mu_B$). The molecular structures of **7** and **8** were established by X-ray diffraction of suitable single-crystals, which were obtained by vapor diffusion of *n*-hexane into a saturated solution of the complexes in toluene (Figure 4). Compound **7** crystallizes in the monoclinic space group *C*2/*c*, complex **8** in the space group $P2_1/c$. Both compounds crystallize with one molecule in the asymmetric unit and adopt a square pyramidal structure with the chloride ligand Cl3 in apical positions and the two other chloride ligands and both carbene ligands in the basis of the pyramid. The Ti–C distances observed for the $cAAC^{Me}$ titanium(III) complex **8** of 2.2991(12) Å and 2.2793(42) Å are slightly shorter than the distances observed for the titanium(IV) complex $[TiCl_4(cAAC^{Me})_2]$ **4** [2.3309(55) Å and 2.3294(55) Å], while the corresponding IMes complexes **2** and **7** show the same distances within experimental error (see Table 3). This difference might be explained by the better acceptor behavior of the $cAAC^{Me}$ ligand[3e] and some delocalization of the $d^1$-electron into the carbene $p_\pi$-orbital ($\pi$-backbonding). The comparison of the $Ti^{III}$ complexes **7** and **8** also reveals the stronger $\pi$-acceptor strength of $cAAC^{Me}$ compared to IMes, which is reflected in different Ti–C1 bond lenths: Ti–C1 2.3268(40) in $[TiCl_3(IMes)_2]$ **7** is significantly longer than Ti–C1 2.2946(33) in $[TiCl_3(cAAC^{Me})_2]$ **8**. On the other hand, the Ti–Cl1/Cl2/Cl3 bond lengths are larger for the complex of the stronger $\sigma$-donor ligand $cAAC^{Me}$ **8**, as the electron density at the titanium center should be increased, which results in a stronger Pauli-repulsion between titanium and the chlorido ligands.

With the three complexes **3**, **4** and **8** in hand, the degree of $\pi$-backdonation from titanium to the adjacent $cAAC^{Me}$ can be put into perspective with another example of a group IV carbene

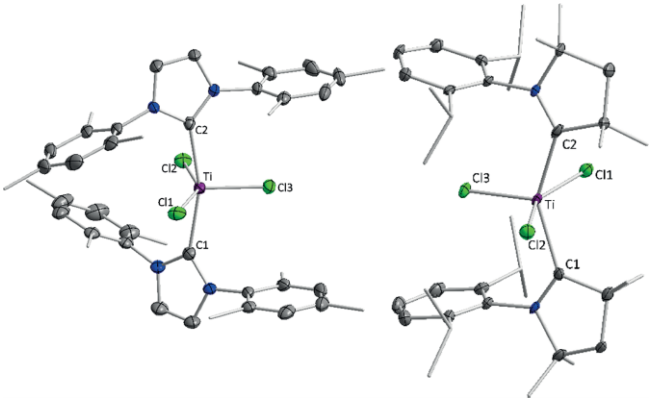


Figure 4. Molecular structures of $[TiCl_3(IMes)_2]$ **7** (left) and $[TiCl_3(cAAC^{Me})_2]$ **8** (right) in the solid state. Hydrogen atoms and a co-crystallized molecule of toluene are omitted for clarity. Atomic displacement ellipsoids are set at 50 % probability. Selected bond lengths [Å] and angles [°] for **7**: Ti–C1 2.3268(40), Ti–C2 2.3379(37), Ti–Cl1 2.3049(14), Ti–Cl2 2.3158(15), Ti–Cl3 2.29991(12), C1–Cl1 3.1244(42), C2–Cl2 3.1946(41), Cl1–Ti–Cl2 147.37(5), Cl2–Ti–Cl3 100.26(5), Cl1–Ti–Cl3 112.35(5), C1–Ti–C2 163.08(14). Selected bond lengths [Å] and angles [°] for **8**: Ti–C1 2.2946(33), Ti–C2 2.2793(42), C1–Cl2 3.1125(38), C2–Cl1 3.0298(38), Ti–Cl1 2.3477(13), Ti–Cl2 2.3612(15), Ti–Cl3 2.2380(15), C1–Ti–C2 147.00(15), C1–Ti–Cl1 89.53(11), 2.29991(12), Cl1–Ti–Cl2 147.37(5), Cl2–Ti–Cl3 100.26(5), Cl3–Ti–Cl1 112.35(5).

complex, namely $[HfCl_2(cAAC^{Me})_2]$ presented by Deng et al., in dependence of its oxidation state +4, +3 and in case of Hf +2. One would expect a gradual increase of the C1–N distance, the more electrons are present for a backdonation into the $p_\pi$-orbital at the carbon atom. This trend is indeed observed by investigation of the corresponding C1–N bond lengths {**3**: 1.299(4) Å, **4**: 1.314(6)/1.297(6) Å, **8**: 1.328(5) Å and $[HfCl_2(cAAC^{Me})_2]$: 1.373(4) Å}.[19a]

To investigate the electronic situation and probe the question whether these complexes are metal centered $d^1$-radical or if the electron is delocalized into the carbene $p_\pi$-orbital, EPR spectra were recorded for both complexes $[TiCl_3(IMes)_2]$ (**7**) and $[TiCl_3(cAAC^{Me})_2]$ (**8**) in the solid (i.e. microcrystalline) state at room temperature (see Figure 5). Corresponding studies in toluene solution led to various decomposition pathways and unreproducible results. The superior $\pi$-accepting character of the $cAAC^{Me}$ (**8**: $g_{iso}$ = 1.973) vs. the IMes ligand (**7**: $g_{iso}$ = 1.945) is reflected in the higher *g* value, which is a result of the reduced unpaired spin density on the titanium atom.[18]

To support the results of the EPR experiments and the magnetometry measurements in solution, the spin densities of the complexes **7** and **8** (Figure 6) were calculated. The resulting spin densities reveal in both cases titanium-centered metalloradicals in which the $d^1$-electron resides in a titanium d-orbital. In order to gain a deeper insight in the electronic situation we also recorded the UV/Vis spectra of both compounds **7** and **8** (Figure 7). Compound **7** reveals two distinct absorption bands at 345 and 597 nm, whereas **8** shows two absorption bands in the same region (358 and 594 nm) and one additional band at 464 nm.

According to TD-DFT calculations, the absorption bands of both complexes at approximately 590 nm can be assigned to d-d-bands, i.e. absorptions from the occupied HOMO into an unoccupied titanium-centered $d_{z^2}$-orbital (*z* is defined perpendicular

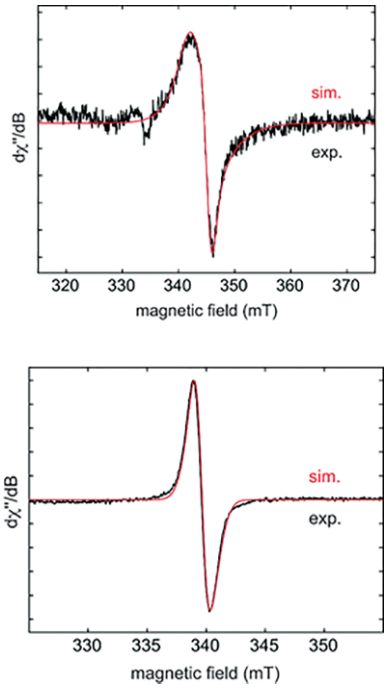


Figure 5. Experimental and anisotropically simulated isotropic continuous-wave (CW) X-band EPR spectra of $[TiCl_3(IMes)_2]$ **7** ($g_{iso}$ = 1.945, top) and $[TiCl_3(cAAC^{Me})_2]$ **8** ($g_{iso}$ = 1.973, bottom) in the solid state at room temperature.

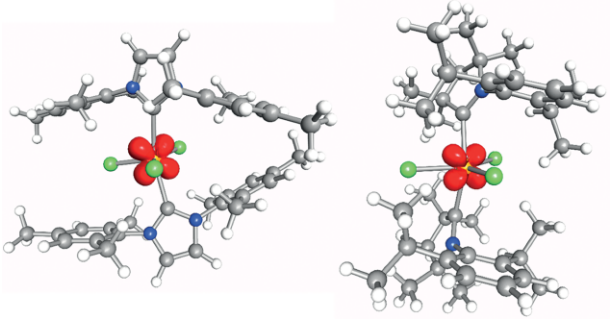

Figure 6. Calculated spin densities of $[TiCl_3(IMes)_2]$ **7** (left) and $[TiCl_3(cAAC^{Me})_2]$ (right) **8** [TURBOMOLE, DFT, PBE0-D3BJ//def2-TZVP(Ti)/def2-SVP].

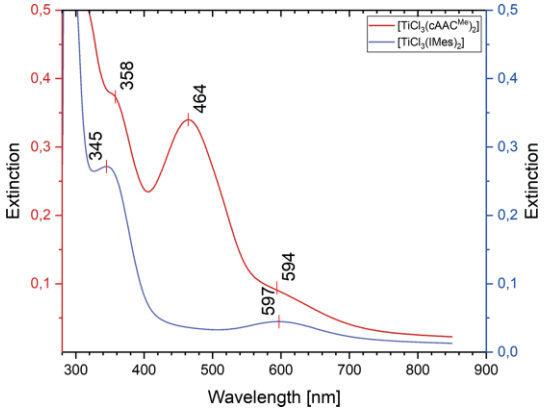


Figure 7. UV/Vis spectra of **7** (blue) and **8** (red) in toluene. Molar extinction coefficients of **7**: $\varepsilon_{597}$ = 29 L mol$^{-1}$ cm$^{-1}$, $\varepsilon_{345}$ = 180 L mol$^{-1}$ cm$^{-1}$. Molar extinction coefficients of **8**: $\varepsilon_{594}$ = 29 L mol$^{-1}$ cm$^{-1}$, $\varepsilon_{467}$ = 98 L mol$^{-1}$ cm$^{-1}$, $\varepsilon_{358}$ = 108 L mol$^{-1}$ cm$^{-1}$.

to the $TiCl_3$-plane). The additional absorption at 464 nm for compound **8** is a metal to ligand transition from the HOMO of the complex into a low lying, unoccupied $cAAC^{Me}$–Ti–$cAAC^{Me}$ π-bonding orbital, which lies much higher in energy for the NHC complex **7**.[19b] The absorption bands of both complexes at ca. 350 nm originate from several intra-ligand transitions.

## Conclusions

In conclusion, we investigated the coordination chemistry of NHC and $cAAC^{Me}$ ligands in chloride complexes of the 3d early transition metal titanium in its highest oxidation states +4 and +3. Starting with calculations of the bond dissociation energies of relevant ligands without additional anchoring groups, we demonstrated that the BDEs of $[TiCl_4(L)_2]$ into 2 L and $[TiCl_4]$ are low in comparison to those typically observed for complexes of late and more electron-rich transition metals. The carbene stabilized titanium(IV) chloride complexes $[TiCl_4(IMes)]$ **1**, $[TiCl_4(IMes)_2]$ **2**, $[TiCl_4(cAAC^{Me})]$ **3**, $[TiCl_4(cAAC^{Me})_2]$ **4** and $[TiCl_4(l\mathit{i}PrMe)]$ **5** are accessible via the direct reaction of the free carbenes with $[TiCl_4]$ or with the mono-carbene complexes, respectively. The mono-carbene complexes are suitable starting materials for mixed ligated complexes, as exemplified by the synthesis of $[TiCl_4(IMes)(PMe_3)]$ **6**. The molecular structures of the complexes **2**–**5** show distinct through-space interactions between the X-ligand p-orbital and the carbene $p_\pi$-orbital (i.e. the chloride ligands point towards the $p_\pi$-orbitals of the carbene carbon atoms). In case of the bis-carbene complexes **2** and **4**, both a second order Jahn–Teller distortion, which strengthens the M–L bond, and a through-space interactions might contribute to the stability of these complexes. This behavior and the molecular structures change drastically in case of the $d^1$ complexes $[TiCl_3(IMes)_2]$ **7** and $[TiCl_3(cAAC^{Me})_2]$ **8**, as the additional electron shows some delocalization into the carbene $p_\pi$-orbitals. Consequently, the M–L distances decrease, and the chloride ligands lie in one plane without forming any intra-ligand interaction. Magnetometry in solution, EPR and UV/Vis spectroscopy and DFT calculations performed on **7** and **8** are indicative of a predominantly metal-centered $d^1$-radical in both cases.

## Experimental Section

### General Considerations

All reactions and subsequent manipulations involving organometallic reagents were performed under an argon atmosphere by using standard Schlenk techniques or in a Glovebox (Innovative Technology Inc. and MBraun Uni Lab) as reported previously.[20] All reactions were carried out in oven-dried glassware. Toluene, *n*-hexane and THF were obtained from a solvent purification system (Innovative Technology). Deuterated benzene was purchased from Sigma-Aldrich, dried with sodium/ketyl and stored over molecular sieve. The carbene ligands l*i*PrMe[21] IMes[22] and $cAAC^{Me}$[2] were prepared according to published procedures. Elemental analyses were performed in the microanalytical laboratory of the University of Würzburg with an Elementar vario micro cube. Infrared spectra were recorded on a Bruker alpha spectrometer as solids by using an ATR unit. The UV/Vis spectra were recorded on a JASCO V-670 spectrophotometer in a sealed cuvette in toluene. NMR spectra were recorded at 298 K using Bruker Avance

400 ($^1$H, 400.4 MHz; $^{13}$C, 100.7 MHz, $^{31}$P, 161.9 MHz) spectrometers. $^1$H NMR chemical shifts are listed in parts per million (ppm), are reported relative to TMS and were referenced via residual proton resonances of the deuterated solvent ($C_6D_5H$: 7.16 ppm). $^{13}C\{^1H\}$ NMR resonances are reported relative to TMS using the natural-abundance carbon resonances of $C_6D_6$ (128.06 ppm).[23] EPR measurements at X-band (9.38 GHz) were carried out using a Bruker ELEXSYS E580 CW/FT EPR spectrometer. The spectral simulations were performed using MATLAB 9.6 (2019a) and the EasySpin 5.2.25 toolbox.[24]

### Synthesis and Characterization of the Compounds

**Synthesis of [$TiCl_4$(IMes)] (1):** A pre-cooled (–78 °C) solution of [$TiCl_4$] (144 µL, 249 mg, 1.31 mmol) in 5 mL *n*-hexane was added to a pre-cooled (–78 °C) solution of IMes (400 mg, 1.31 mmol) in 15 mL *n*-hexane. The mixture was warmed up to room temperature within 4 h and was then stirred for additional 72 h at room temperature. The yellow precipitate formed during this process was filtered off, washed with *n*-hexane (4 × 5 mL portions) and the remaining solid was dried in vacuo. Yield: 478 mg (967 µmol, 74 %) of a pale yellow solid. $^1$H NMR (400.1 MHz,$C_6D_6$, 25 °C): 2.01 (s, 6 H, aryl-C$H_{3para}$), 2.21 (s, 12 H, aryl-C$H_{3ortho}$), 5.85 (s, 2 H, C*H*C*H*), 6.68 (s, 4 H, aryl-C$H_{3meta}$) ppm. $^{13}C\{^1H\}$ NMR (100.6 MHz, $C_6D_6$, 25 °C): 19.1 (aryl-$CH_{3ortho}$), 21.0 (aryl-$CH_{3para}$), 122.1 (*C*HCH), 129.9 (aryl-$C_{meta}$), 133.1 (aryl-$C_{ortho}$), 136.0 (aryl-$C_{ipso}$), 140.6 (aryl-$C_{para}$), 186.4 (NCN) ppm. IR (ATR [$cm^{-1}$]): 436 (vs), 477 (m), 558 (w), 701 (m), 748 (s), 854 (m), 922 (vw), 1017 (vw), 1112 (vw), 1229 (w), 1380 (vw), 1403 (vw), 1464 ($vw_{br}$ ), 1480 ($vw_{br}$ ), 1611 (vw), 2916 (vw), 3162 (vw), 3172 (vw). $C_{21}H_{24}Cl_4N_2Ti$ (494.10 g/mol): calcd.: C 51.05, H 4.90, N 5.67; found C 51.23, H 5.05, N 5.57.

**Synthesis of [$TiCl_4$(IMes)$_2$] (2):** A suspension of [$TiCl_4$(IMes)] **1** (162 mg, 328 µmol) in 5 mL *n*-hexane was added to a suspension of IMes (100 mg, 328 µmol) in 5 mL *n*-hexane. The mixture was stirred for additional 16 h at room temperature. The yellow precipitate formed during the reaction was filtered off, washed with *n*-hexane (4 × 5 mL portions) and the remaining solid was dried in vacuo. Yield: 233 mg (292 µmol, 89 %) of a yellow solid. $^1$H NMR (400.1 MHz, $C_6D_6$, 25 °C): 2.10 (s, 6 H, aryl–C$H_{3para}$), 2.27 (s, 12 H, aryl-C$H_{3ortho}$), 5.91 (s, 2H, C*H*C*H*), 6.67 (s, 4 H, ary-C$H_{3meta}$) ppm. $^{13}C\{^1H\}$ NMR (100.6 MHz, $C_6D_6$, 25 °C): 19.2 (aryl-$CH_{3ortho}$), 21.2 (aryl-$CH_{3para}$), 122.4 (*C*HCH), 128.8 (aryl-$C_{meta}$), 136.2 (aryl-$C_{ortho}$), 137.9 (aryl-$C_{ipso}$), 138.1 (aryl-$C_{para}$), 190.1 (NCN) ppm. IR (ATR [$cm^{-1}$]): = 469 (w), 577 (w), 640 (w), 695 (vs), 738 (vs), 848 (vs), 861 (s), 926 (s), 1016 (w), 1034 (w), 1099 (w), 1211 (w), 1258 (s), 1389 (s), 1464 (s), 1485 (w), 2851 (w), 2916 (w). $C_{42}H_{48}Cl_4N_4Ti{\bullet}C_7H_8$ (890.68 g/mol): calcd.: 66.09, H 6.34, N 6.29; found C 66.08, H 6.45, N 6.27.

**Synthesis of [$TiCl_4$(cAAC$^{Me}$)] (3):** A pre-cooled (–78 °C) solution of cAAC$^{Me}$ (300 mg, 1.05 mmol) in 10 mL *n*-hexane was added to a pre-cooled (–78 °C) solution of [$TiCl_4$] (115 µL, 199 mg, 1.05 mmol) in 5 mL *n*-hexane. The mixture was warmed up to room temperature within 4 h and was stirred over a period of an additional 72 h at room temperature. The yellow precipitate formed during this process was filtered off, was washed with *n*-hexane (4 × 5 mL) and the remaining solid was dried in vacuo. Yield: 416 mg (876 µmol, 84 %), dark yellow solid. $^1$H NMR (400.1 MHz, $C_6D_6$, 25 °C): 0.81 (s, 6 H, NC($CH_3$)$_2$), 1.08 (d, 6 H, $^3J_{HH}$ = 6.4 Hz, CH($CH_3$)$_2$), 1.35 (s, 2 H, $CH_2$), 1.53 (d, 6H, $^3J_{HH}$ = 6.4 Hz, CH($CH_3$)$_2$), 1.58 (s, 6 H, N($C_2$($CH_3$)$_2$)), 3.03 (sept, 2 H, $^3J_{HH}$ = 6.4 Hz, *C*H($CH_3$)$_2$), 6.98–7.06 (m, 3 H, Ar–C*H*) ppm. $^{13}C\{^1H\}$ NMR (100.6 MHz, $C_6D_6$, 25 °C): 25.8 [CH($CH_3$)$_2$], 28.4 [CH($CH_3$)$_2$], 29.2 (NC($CH_3$)$_2$), 29.4 [CH($CH_3$)$_2$] 32.2 ($CH_2$C($CH_3$)$_2$), 52.1 ($CH_2$), 54.1 (CC($CH_3$)$_2$), 82.4 (NC($CH_3$)$_2$), 126.1 (aryl–$CH_{meta}$), 130.3 (aryl-$CH_{para}$), 133.2 (aryl-$C_{ipso}$), 146.1 (aryl-$C_{ortho}$), 260.3 (NCC($CH_3$)$_2$) ppm. IR (ATR [$cm^{-1}$]): 412 (vs), 445 (m), 463 (w), 563 (vw), 775 (m), 810 (m), 1105 (vw), 1124 (vw), 1193 (vw), 1373 (w), 1389 (w), 1460 (w), 1509 (w), 2974 (w), 2990 (w). $C_{20}H_{31}Cl_4NTi$ (475.14 g/mol): calcd.: C 50.56; H 6.58, N 2.95; found C 50.23, H 6.67, N 2.78.

**Synthesis of [$TiCl_4$(cAAC$^{Me}$)$_2$] (4):** A pre-cooled (–78 °C) solution of cAAC$^{Me}$ (300 mg, 1.05 mmol) in 10 mL *n*-hexane was added to a pre-cooled (–78 °C) solution of [$TiCl_4$] (57.6 µL, 99.7 mg, 525 mmol) in *n*-hexane. The mixture was warmed up to room temperature in 4 h and was stirred over a period of an additional 72 h. The bright red precipitate formed during this process was filtered off and was washed with *n*-hexane (2 × 5 mL) and the solid was dried in vacuo. Yield: 227 mg (479 µmol, 91 %), red solid. $^1$H NMR (400.1 MHz, $C_7D_8$, 0 °C): 0.99 (s, 6 H, NC($CH_3$)$_2$), 1.27 (d, 6 H, $^3J_{HH}$ = 6.5 Hz, CH($CH_3$)$_2$), 1.53 (s, 2 H, $CH_2$), 1.73 (d, 6 H, $^3J_{HH}$ = 6.5 Hz, CH($CH_3$)$_2$), 1.81 (s, 6 H, C($CH_3$)$_2$), 3.24 (sept, 2 H, $^3J_{HH}$ = 6.5 Hz, *C*H($CH_3$)$_2$), 6.72–6.77 (m, 2 H, (Ar-C*H*)), 6.91 (d, 2 H, (Ar-C*H*)) ppm. $^{13}C\{^1H\}$ NMR (100.6 MHz, $C_7D_8$, 0 °C): 24.2 [CH($CH_3$)$_2$], 29.1 [CH($CH_3$)$_2$], 29.2 [CH($CH_3$)$_2$], 29.4 ($CH_2$C($CH_3$)$_2$), 31.6 ($CH_2$C($CH_3$)$_2$), 56.6 ($CH_2$), 80.4 (NC($CH_3$)$_2$), 124.4 (aryl-$CH_{para}$), 129.6 (aryl-$CH_{meta}$), 135.5 (aryl-$C_{ipso}$), 146.4 (aryl-$C_{ortho}$), 264.2 (NCC($CH_3$)$_2$) ppm. IR (ATR [$cm^{-1}$]): 414 (w), 447 (w), 465 (w), 565 (w), 769 (s), 806 (s), 1126 (w), 1187 (w), 1371 (m), 1387 (m), 1456 (s), 2867 (m), 2929 (m), 2949 (m), 2961 (w). $C_{40}H_{62}Cl_4N_2Ti$ (760.61 /mol): calcd.: C 63.16, N 8.22, H 3.68; found C 62.94, H 8.65, N 3.34.

**Synthesis of [$TiCl_4$(*li*PrMe)] (5):**[9] A pre-cooled (–78 °C) suspension of l*i*PrMe (250 mg, 1.37 mmol) in 15 mL *n*-hexane was added to a pre-cooled (–78 °C) solution of [$TiCl_4$] (265 µL, 458 mg, 1.37 mmol) in 5 mL *n*-hexane. The mixture was warmed up to room temperature in 4 h and was stirred over a period of an additional 72 h. The red precipitate was filtered off and was washed with *n*-hexane (4 × 5 mL) and the solid was dried in vacuo. Yield: 405 mg (1.09 mmol, 80 %), red solid. $^1$H NMR (400.1 MHz, $C_6D_6$, 25 °C): 1.07 (s, 12 H, CH($CH_3$)$_2$), 1.37 (s, 6 H, NCC$H_3$CC$H_3$N), 4.76 (sept, 2 H, *C*H($CH_3$)$_2$) ppm. $^{13}C\{^1H\}$ NMR (100.6 MHz, $C_6D_6$, 25 °C): 9.9 (NCC$H_3$CC$H_3$N), 20.8 [CH($CH_3$)$_2$], 53.9 [*C*H($CH_3$)$_2$], 124.5 (NC*C*H$_3$C*C*H$_3$N), 185.3 (NCN) ppm. IR (ATR [$cm^{-1}$]): 441 (vs), 540 (m), 751 (m), 810 (w), 894 (w), 1102 (m), 1137 (m), 1199 (m), 1224 (w), 1322 (m), 1340 (m), 1368 (m), 1385 (w), 1399 (m), 1632 (w), 2940 (m), 2975 (m).

**Synthesis of [$TiCl_4$(IMes)($PMe_3$)] (6):** $PMe_3$ (50µL, 30.8 mg, 405 µmol) was added at room temperature to a suspension of **1** (200 mg, 405 µmol) in 10 mL *n*-hexane and was stirred for 10 minutes. A red precipitate formed starting with the addition of the phosphine, which was filtered off and was washed with *n*-hexane (3 × 5 mL). The remaining solid was dried in vacuo. Yield: 163 mg (287 µmol, 71 %), bright red solid. $^1$H NMR (400.1 MHz, $C_6D_6$, 25 °C): 1.04 (s, 9 H, P($CH_3$)$_3$), 2.13 (s, 6 H, aryl-C$H_{3para}$), 2.34 (s, 12 H, aryl-C$H_{3meta}$), 6.02 (s, 2 H, NC*H*C*H*N), 6.80 (s, 4 H, aryl-C$H_{meta}$) ppm. $^{13}C\{^1H\}$ NMR (100.6 MHz, $C_6D_6$, 25 °C): 15.7 ($^1J_{CP}$ = 20.5 Hz, P($CH_3$)$_3$), 18.7 (aryl-$CH_{3ortho}$), 21.1 (aryl-$CH_{3para}$), 122.4 (*C*HCH), 129.9 (aryl-$CH_{meta}$), 136.2 (aryl-$CH_{3ortho}$), 137.4 (aryl-$C_{ipso}$), 139.0 (aryl-$CCH_{3para}$), 190.4 (NCN) ppm. $^{31}$P NMR (161.9 MHz, $C_6D_6$, 25 °C): –8.05 ppm. $C_{24}H_{33}Cl_4N_2PTi$ (570.18 g/mol): calcd.: C 50.56, H 5.83, N: 4.91; found C 50.67, H 6.19, N 4.92.

**Synthesis of [$TiCl_3$(IMes)$_2$] (7):** A pre-cooled (–78 °C) suspension of [$TiCl_3$(THF)$_3$] (304 mg, 821 µmol) in 5 mL *n*-hexane was added to a pre-cooled (–78 °C) suspension of IMes (500 mg, 1.64 mmol) in 10 mL *n*-hexane. The mixture was warmed up to room temperature in 4 h and was stirred over a period of 16 h. A colour change from green to blue could be observed. The precipitate was filtered off and washed with *n*-hexane (3 × 5 mL) and was dried in vacuo. Yield: 528 mg (821 µmol, 84 %), blue solid. Magnetic Moment (Evans-Method):[25] $\mu_{eff}$ = 1.74 $\mu_B$ EPR (Toluene, 70K): $g$ = 1.966. UV/Vis (Toluene, [nm]): 345 ($\varepsilon$ = 180 L $mol^{-1}$ $cm^{-1}$), 597 ($\varepsilon$ = 29 L $mol^{-1}$ $cm^{-1}$). IR (ATR [$cm^{-1}$]): 471 (vw), 575 (w), 642 (vw), 689 (w), 732 (w), 753 (w),

846 (s), 926 (w), 1034 (vw), 1095 (vw), 1260 (w), 1389 (w), 1458 (wbr), 1485 (w), 1976 (vw ), 2035 (vw), 2158 (w), 2914 (w). $C_{42}H_{48}Cl_3N_4Ti$ (761.24 g/mol): calcd.: C 66.11, H 6.34, N 7.34; found C 66.01, H 6.80, N 6.89.

**Synthesis of $[TiCl_3(cAAC^{Me})_2]$ (8):** A pre-cooled (–78 °C) suspension of $[TiCl_3(THF)_3]$ (162 mg, 438 µmol) in 5 mL *n*-hexane was added to a pre-cooled (–78 °C) suspension of $cAAC^{Me}$ (525 mg, 876 µmol) in 10 mL *n*-hexane. The mixture was warmed up to room temperature in 4 h and was stirred over a period of 16 h. A colour change from green over colourless to deep violet was observed. The precipitate was filtered off and washed with *n*-hexane (3 × 5 mL) and *n*-pentane (3 × 5 mL) and was dried in vacuo. Yield: 190 mg (262 µmol, 60 %), violet solid. Magnetic Moment (Evans-Method):[25] $\mu_{eff}$ = 2.47 $\mu_B$ EPR (Toluene, 70K): $g$ = 1.971. UV/Vis (Toluene, [nm]): 358 ($\varepsilon$ = 108 L mol$^{-1}$ cm$^{-1}$), 464 ($\varepsilon$ = 98 L mol$^{-1}$ cm$^{-1}$), 594 ($\varepsilon$ = 26 L mol$^{-1}$ cm$^{-1}$). IR (ATR [cm$^{-1}$]): 404 (vw), 416 (vw), 492 (w), 567 (w), 771 (vs), 808 (vs), 1050 (w), 1128 (m), 1195 (m), 1371 (m), 1389 (m), 1456 (vs), 2925 (m), 2963 (m), 2984 (m). $C_{40}H_{62}Cl_3N_2Ti$ (725.16 g/mol): calcd.: C 66.25, H 8.62, N 3.86; found C 66.56, H 9.13, N 3.87.

### Crystallographic Details

Crystal data collection and processing parameters are given in Table SI1 – SI2 (see SI). Crystals were immersed in a film of perfluoropolyether oil on a glass fiber MicroMount™ (MiTeGen) and transferred to a Bruker D8 Apex-1 diffractometer with CCD area detector and graphite-monochromated Mo-$K_\alpha$ radiation or a Bruker D8 Apex-2 diffractometer with CCD area detector and graphite-monochromated Mo-$K_\alpha$ radiation equipped with an Oxford Cryosystems low-temperature device or a Rigaku XtaLAB Synergy-DW diffractometer with HyPix-6000HE detector and monochromated Cu-$K_\alpha$ equipped with an Oxford Cryo 800 cooling unit. Data were collected at 100 K. The images were processed with the Bruker or Crysalis software packages and equivalent reflections were merged. Corrections for Lorentz-polarization effects and absorption were performed if necessary and the structures were solved by direct methods. Subsequent difference Fourier syntheses revealed the positions of all other non-hydrogen atoms. The structures were solved by using the ShelXTL software package.[26] All non-hydrogen atoms were refined anisotropically. Hydrogen atoms were usually assigned to idealized positions and were included in structure factors calculations. In case of the molecular structures **4** and **7** the squeeze function was used to include a disordered benzene solvent molecule into the model.

CCDC 1964330 (for **2**), 1964332 (for **3**), 1964334 (for **4**), 1964335 (for **5**), 1964333 (for **7**), and 1964331 (for **8**) contain the supplementary crystallographic data for this paper. These data can be obtained free of charge from The Cambridge Crystallographic Data Centre.

**Experimental Crystal Data Collection of $[TiCl_4(IMes)_2]$ (2):** $C_{48}H_{54}Cl_4N_4Ti$, $M_r$ = 438.32, $T$ = 100.00(10) K, wavelength = 0.71073 Å, triclinic space group $P2_1/n$, $a$ = 12.4326(17) Å, $b$ = 12.5681(17) Å, $c$ = 15.401(2) Å, $\alpha$ = 75.974(4)°, $\beta$ = 82.031(4)°, $\gamma$ = 75.688(4)°, $V$ = 2254.3(5) Å$^3$, Z = 4, $\rho(calcd)$ = 1.292 g/cm$^3$, $\mu$ = 0.465 mm$^{-1}$, $F$(000) = 920, 33524 reflections in $-16 \le h \le 16$, $-16 \le k \le 16$, $-20 \le l \le 20$ measured in $1.368 < \nu < 28.336°$, completeness 99.5 %, 11210 independent reflections, 9071 reflections observed in [$I$ > 2sigma($I$)], 526 parameters, 0 restraints, $R$ indices (all data) $R_1$ = 0.0514, $wR_2$ = 0.0908, final $R$ indices [$I$ > 2sigma($I$)] $R_1$ = 0.0379, $wR_2$ = 0.0852, largest difference peak and hole 0.498 and –0.428 eA$^{-3}$, GooF = 1.025.

**Experimental Crystal Data Collection of $[TiCl_4(cAAC^{Me})]$ (3):** $C_{20}H_{31}Cl_4NTi$, $M_r$ = 475.16, $T$ = 100.00(10) K, wavelength = 0.71073Å, orthorhombic space group $P2_12_12_1$, $a$ = 10.1592(6) Å, $b$ = 14.9109(9) Å, $c$ = 14.9422(7) Å, $\alpha$ = 90°, $\beta$ = 90°, $\gamma$ = 90°, $V$ = 2263.5(2) Å$^3$, Z = 4, $\rho(calcd)$ = 1.394 g/cm$^3$, $\mu$ = 0.855 mm$^{-1}$, $F$(000) = 992, 9938 reflections in $-12 \le h \le 7$, $-18 \le k \le 18$, $-16 \le l \le 12$ measured in $1.929 < \nu < 26.050°$, completeness 96.6 %, 4290 independent reflections, 9597 reflections observed in [$I$ > 2sigma($I$)], 243 parameters, 0 restraints, $R$ indices (all data) $R_1$ = 0.0323, $wR_2$ = 0.0760 final $R$ indices [$I$ > 2sigma($I$)] $R_1$ = 0.0304, $wR_2$ = 0.0751, largest difference peak and hole 0.430 and –0.308 eA$^{-3}$, GooF = 1.035.

**Experimental Crystal Data Collection of $[TiCl_4(cAAC^{Me})_2]$ (4):** $C_{43}H_{69}Cl_4N_2Ti$, $M_r$ = 803.70, $T$ = 100.00(10) K, wavelength = 0.71073 Å, triclinic space group P1$^-$, $a$ = 11.681(5) Å, $b$ = 12.031(5) Å, $c$ = 17.135(7) Å, $\alpha$ = 102.826(17)°, $\beta$ = 101.092(16)°, $\gamma$ = 105.881(16)°, $V$ = 2174.6(16) Å$^3$, Z = 2, $\rho(calcd)$ = 1.227 g/cm$^3$, $\mu$ = 0.474 mm$^{-1}$, $F$(000) = 862, 29182 reflections in $-14 \le h \le 14$, $-14 \le k \le 14$, $-21 \le l \le 21$ measured in $1.839 < \nu < 26.362°$, completeness 99.2 %, 8648 independent reflections, 4456 reflections observed in [$I$ > 2sigma($I$)], 456 parameters, 36 restraints, $R$ indices (all data) $R_1$ = 0.1720, $wR_2$ = 0.1682 final $R$ indices [$I$ > 2sigma($I$)] $R_1$ = 0.0799, $wR_2$ = 0.1425, largest difference peak and hole 0.607 and –0.794 eA$^{-3}$, GooF = 1.010. The squeeze function was used for the structural analysis of compound **7** to include a disordered benzene solvent molecule into the model.

**Experimental Crystal Data Collection of $[TiCl_4(IiPrMe)]$ (5):** $C_{11}H_{20}Cl_4N_2Ti$, $M_r$ = 369.99, $T$ = 100.00(10) K, wavelength = 0.71073Å, monoclinic space group $P2_1/n$, $a$ = 8.8788(3) Å, $b$ = 13.2025(4) Å, $c$ = 14.8596(5) Å, $\alpha$ = 90°, $\beta$ = 91.126(2)°, $\gamma$ = 90°, $V$ = 1741.54(10) Å$^3$, Z = 4, $\rho(calcd)$ = 1.411 g/cm$^3$, $\mu$ = 1.091 mm$^{-1}$, $F$(000) = 760, 23884 reflections in $-11 \le h \le 11$, $-16 \le k \le 16$, $-18 \le l \le 18$ measured in $2.064 < \nu < 26.911°$, completeness 99.7 %, 3754 independent reflections, 3400 reflections observed in [$I$ > 2sigma($I$)], 169 parameters, 0 restraints, $R$ indices (all data) $R_1$ = 0.0262, $wR_2$ = 0.0516 final $R$ indices [$I$ > 2sigma($I$)] $R_1$ = 0.0222, $wR_2$ = 0.0492, largest difference peak and hole 0.322 and –0.343 eA$^{-3}$, GooF = 0.811.

**Experimental Crystal Data Collection of $[TiCl_3(IMes)_2]$ (7):** $C_{42}H_{48}Cl_3N_4Ti$, $M_r$ = 763.09, $T$ = 100.00(10) K, wavelength = 0.71073Å, monoclinic space group $C2/c$, $a$ = 30.0391(8) Å, $b$ = 12.9222(3) Å, $c$ = 24.0767(5) Å, $\alpha$ = 90°, $\beta$ = 99.3660(10)°, $\gamma$ = 90°, $V$ = 9221.3(4) Å$^3$, Z = 8, $\rho(calcd)$ = 1.099 g/cm$^3$, $\mu$ = 0.385 mm$^{-1}$, $F$(000) = 3208, 29019 reflections in $-36 \le h \le 36$, $-15 \le k \le 15$, $-26 \le l \le 26$ measured in $2.064 < \nu < 26.911°$, completeness 98.3 %, 8943 independent reflections, 7125 reflections observed in [$I$ > 2sigma($I$)], 463 parameters, 0 restraints, $R$ indices (all data) $R_1$ = 0.0469, $wR_2$ = 0.0884 final $R$ indices [$I$ > 2sigma($I$)] $R_1$ = 0.0334, $wR_2$ = 0.0818, largest difference peak and hole 0.324 and –0.343 eA$^{-3}$, GooF = 1.009. The squeeze function was used for the structural analysis of compound **7** to include a disordered benzene solvent molecule into the model.

**Experimental Crystal Data Collection of $[TiCl_3(cAAC^{Me})_2]$ (8):** $C_{40}H_{62}Cl_3N_2Ti$, $M_r$ = 362.58, $T$ = 100.00(10) K, wavelength = 0.71073Å, monoclinic space group $P2_1/c$, $a$ = 20.560(4) Å, $b$ = 11.5713(19) Å, $c$ = 17.753(3) Å, $\alpha$ = 90°, $\beta$ = 108.425(6)°, $\gamma$ = 90°, $V$ = 4007.0(12) Å$^3$, Z = 8, $\rho(calcd)$ = 1.202 g/cm$^3$, $\mu$ = 0.442 mm$^{-1}$, $F$(000) = 1556, 40719 reflections in $-25 \le h \le 25$, $-14 \le k \le 14$, $-21 \le l \le 21$ measured in $2.046 < \nu < 26.129°$, completeness 99.4 %, 7938 independent reflections, 4116 reflections observed in [$I$ > 2sigma($I$)], 431 parameters, 0 restraints, $R$ indices (all data) $R_1$ = 0.1513, $wR_2$ = 0.1530 final $R$ indices [$I$ > 2sigma($I$)] $R_1$ = 0.0632, $wR_2$ = 0.1193, largest difference peak and hole 0.451 and –0.503 eA$^{-3}$, GooF = 0.966.

### Computational Details

Calculations have been performed using the TURBOMOLE V7.2 program suite, a development of University of Karlsruhe and the Forschungszentrum Karlsruhe GmbH, 1989–2007, TURBOMOLE GmbH, since 2007; available from http://www.turbomole.com.[27] Geometry optimizations were performed using (RI-)DFT calculations[28] on a m4 grid employing the BP86[29] functional and a def2-TZVP basis set for titanium and for all other atoms the def2-SVP basis sets.[30] Vibrational frequencies were calculated at the same level with the AOFORCE[31] module and all structures represented true minima without imaginary frequencies. TD-DFT calculations were carried out for the first 30 singlet and triplet excited states employing the same basis sets employing the PBE0[32] functional together with Grimme's empirical dispersion correction (D3BJ).[33] Representations of molecular orbitals were produced with the TmoleX graphical interface. Cartesian coordinates of the compounds are provided in the SI.

## Acknowledgments

This work was supported by the Julius-Maximilians-University Würzburg and the Deutsche Forschungsgemeinschaft (DFG).

**Keywords:** N–Heterocyclic carbenes · Carbene ligands · Titanium · Structure elucidation

[1] A. J. Arduengo III, R. L. Harlow, M. Kline, *J. Am. Chem. Soc.* **1991**, *113*, 361–363.
[2] V. Lavallo, Y. Canac, C. Präsang, B. Donnadieu, G. Bertrand, *Angew. Chem. Int. Ed.* **2005**, *44*, 5705–5709; *Angew. Chem.* **2005**, *117*, 5851–5855.
[3] a) M. Melaimi, M. Soleilhavoup, G. Bertrand, *Angew. Chem. Int. Ed.* **2010**, *49*, 8810–8849; *Angew. Chem.* **2010**, *122*, 8992–9032; b) M. Soleilhavoup, G. Bertrand, *Acc. Chem. Res.* **2015**, *48*, 256–266; c) S. Roy, K. C. Mondal, H. W. Roesky, *Acc. Chem. Res.* **2016**, *49*, 357–369; d) M. Melaimi, R. Jazzar, M. Soleilhavoup, G. Bertrand, *Angew. Chem. Int. Ed.* **2017**, *56*, 10046–10068; *Angew. Chem.* **2017**, *129*, 10180; e) U. S. Paul, U. Radius, *Eur. J. Inorg. Chem.* **2017**, 3362–3375; f) U. S. Paul, M. J. Krahfuß, U. Radius, *Chem. Unserer Zeit* **2019**, *53*, 212–223; g) S. Kundu, S. Sinhababu, V. Chandrasekhar, H. W. Roesky, *Chem. Sci.* **2019**, *10*, 4727–4741.
[4] a) C. S. Cazin, *Dalton Trans.* **2013**, *42*, 7254–7254; b) P. de Fremont, N. Marion, S. P. Nolan, *Coord. Chem. Rev.* **2009**, *253*, 862–892; c) S. Diez-Gonzalez, N. Marion, S. P. Nolan, *Chem. Rev.* **2009**, *109*, 3612–3676; d) F. Glorius (ed.), *N-heterocyclic Carbenes in Transition Metal Catalysis*, Springer **2007** ; e) S. Díez-González (ed.), *N-heterocyclic carbenes: from laboratory to curiosities to efficient synthetic tools*, RSC Publishing **2011**; f) F. E. Hahn, M. C. Jahnke, *Angew. Chem. Int. Ed.* **2008**, *47*, 3122–3172; *Angew. Chem.* **2008**, *120*, 3166–3216; g) W. A. Herrmann, *Angew. Chem. Int. Ed.* **2002**, *41*, 1290–1309; *Angew. Chem.* **2002**, *114*, 1342–1363; h) S. P. Nolan, *N-Heterocyclic carbenes in synthesis*, John Wiley & Sons, **2006**; i) S. P. Nolan, *N-Heterocyclic Carbenes: Effective Tools for Organometallic Synthesis*, John Wiley & Sons, **2014**; j) M. Poyatos, J. A. Mata, E. Peris, *Chem. Rev.* **2009**, *109*, 3677–3707; k) T. Rovis, S. P. Nolan, *Synlett* **2013**, *24*, 1188–1189; l) A. A. Danopoulos, T. Simler, P. Braunstein, *Chem. Rev.* **2019**, *119*, 3730–3961.
[5] a) C. M. Crudden, D. P. Allen, *Coord. Chem. Rev.* **2004**, *248*, 2247–2273; b) D. Enders, O. Niemeier, A. Henseler, *Chem. Rev.* **2007**, *107*, 5606–5655; c) M. Fevre, J. Pinaud, Y. Gnanou, J. Vignolle, D. Taton, *Chem. Soc. Rev.* **2013**, *42*, 2142–2172; d) D. M. Flanigan, F. Romanov-Michailidis, N. A. White, T. Rovis, *Chem. Rev.* **2015**, *115*, 9307–9387; e) S. Würtemberger-Pietsch, U. Radius, T. B. Marder, *Dalton Trans.* **2016**, *45*, 5880–5895; f) V. Nair, S. Bindu, V. Sreekumar, *Angew. Chem. Int. Ed.* **2004**, *43*, 5130–5135; *Angew. Chem.* **2004**, *116*, 5240–5245.
[6] a) K. R. Jain, W. A. Herrmann, F. E. Kühn, *Curr. Org. Chem.* **2008**, *12*, 1468–1478; b) D. Zhang, G. Zi, *Chem. Soc. Rev.* **2015**, *44*, 1898–1921; c) J. Cheng, L. Wang, P. Wang, L. Deng, *Chem. Rev.* **2018**, *118*, 9930–9987; d) S. Bellemin-Laponnaz, S. Dagorne, *Chem. Rev.* **2014**, *114*, 8747–8774; e) S. Hameury, P. de Fremont, P. Braunstein, *Chem. Soc. Rev.* **2017**, *46*, 632–733.
[7] a) H. Jacobsen, A. Correa, C. Costabile, L. Cavallo, *J. Organomet. Chem.* **2006**, *691*, 4350–4358; b) R. Tonner, G. Heydenrych, G. Frenking, *Chem. Asian J.* **2007**, *2*, 1555–1567; c) U. Radius, F. M. Bickelhaupt, *Organometallics* **2008**, *27*, 3410–3414; d) H. Jacobsen, A. Correa, A. Poater, C. Costabile, L. Cavallo, *Coord. Chem. Rev.* **2009**, *253*, 687–703; e) J. C. Bernhammer, G. Frison, H. V. Huynh, *Chem. Eur. J.* **2013**, *19*, 12892–12905.
[8] a) M. Kaupp, "Periodizität und fortgeschrittene Aspekte der chemischen Bindung" in *Anorganische Chemie – Prinzipien von Struktur und Reaktivität*, (Eds.: R. Steudel, J. E. Huheey, E. A. Keiter, R. Keiter), de Gruyter, Berlin **2014**, chapter 18; b) M. Kaupp, *J. Comput. Chem.* **2007**, *28*, 320–325.
[9] a) W. A. Herrmann, K. Öfele, M. Elison, F. E. Kühn, P. W. Roesky, *J. Organomet. Chem.* **1994**, *480*, c7–c9; b) N. Kuhn, T. Kratz, D. Bläser, R. Boese, *Inorg. Chim. Acta* **1995**, *238*, 179–181.
[10] F. E. Hahn, T. von Fehren, R. Fröhlich, *Z. Naturforsch. B* **2004**, *59*, 348–350.
[11] P. Shukla, J. A. Johnson, D. Vidovic, A. H. Cowley, C. D. Abernethy, *Chem. Commun.* **2004**, 360–361.
[12] G. B. Nikiforov, H. W. Roesky, P. G. Jones, J. Magull, A. Ringe, R. B. Oswald, *Inorg. Chem.* **2008**, *47*, 2171–2179.
[13] A. Doddi, C. Gemel, R. W. Seidel, M. Winter, R. A. Fischer, *Polyhedron* **2013**, *52*, 1103–1108.
[14] a) C. Lorber, L. Vendier, *Dalton Trans.* **2009**, 6972–6984; b) J. Li, C. Schulzke, S. Merkel, H. W. Roesky, P. P. Samuel, A. Döring, D. Stalke, *Z. Anorg. Allg. Chem.* **2010**, *636*, 511–514.
[15] C. D. Abernethy, G. M. Codd, M. D. Spicer, M. K. Taylor, *J. Am. Chem. Soc.* **2003**, *125*, 1128–1129.
[16] P. Kubacek, R. Hoffmann, *J. Am. Chem. Soc.* **1981**, *103*, 4320–4332.
[17] M. Niehues, G. Kehr, G. Erker, B. Wibbeling, R. Fröhlich, O. Blacque, H. Berke, *J. Organomet. Chem.* **2002**, *663*, 192–203.
[18] B. Goodman, J. Raynor, in *Advances in inorganic chemistry and radiochemistry, Vol. 13*, Elsevier, **1970**, pp. 135–362.
[19] a) Q. Liu, Q. Chen, X. Leng, Q.-H. Deng, L. Deng, *Organometallics* **2018**, *37*, 4186–4188; b) Briefly before submission of our manuscript we became aware of a paper which reports on the formation of a titanium(II) complex $[TiCl_2(cAAC^{Me})_2]$, where in principle this orbital gets populated: W. Ma, J.-X. Zhang, Z. Lin, T. D. Tilley, Q. Ye, *Dalton Trans.* **2019**, *48*, 14962–14965.
[20] J. H. Berthel, L. Tendera, M. W. Kuntze-Fechner, L. Kuehn, U. Radius, *Eur. J. Inorg. Chem.* **2019**, *2019*, 3061–3072.
[21] T. Schaub, U. Radius, A. Brucks, M. P. Choules, M. T. Olsen, T. Rauchfuss, *Inorg. Synth.* **2010**, *35*, 78–91.
[22] A. J. Arduengo, H. V. R. Dias, R. L. Harlow, M. Kline, *J. Am. Chem. Soc.* **1992**, *114*, 5530–5534.
[23] G. R. Fulmer, A. J. Miller, N. H. Sherden, H. E. Gottlieb, A. Nudelman, B. M. Stoltz, J. E. Bercaw, K. I. Goldberg, *Organometallics* **2010**, *29*, 2176–2179.
[24] S. Stoll, A. Schweiger, *J. Magn. Reson.* **2006**, *178*, 42–55.
[25] D. Evans, *J. Chem. Soc.* **1959**, 2003–2005.
[26] G. M. Sheldrick, *Acta Crystallogr., Sect. A* **2015**, *71*, 3–8.
[27] a) F. Furche, R. Ahlrichs, C. Hättig, W. Klopper, M. Sierka, F. T. Weigend, *WIREs Comput. Mol. Sci.* **2014**, *4*, 91–100; b) R. Ahlrichs, M. Bär, M. Häser, H. Horn, C. Kölmel, *Chem. Phys. Lett.* **1989**, *162*, 165–169.
[28] a) O. Treutler, R. Ahlrichs, *J. Chem. Phys.* **1995**, *102*, 346–354; b) M. Häser, R. Ahlrichs, *J. Comput. Chem.* **1989**, *10*, 104–111.
[29] a) A. D. Becke, *Phys. Rev. A* **1988**, *38*, 3098–3100; b) J. Perdew, *Phys. Rev. B* **1986**, *33*, 8822-8824, erratum: *Phys. Rev. B* **1986**, *34*, 7406. .
[30] a) A. Schäfer, H. Horn, R. Ahlrichs, *J. Chem. Phys.* **1992**, *97*, 2571–2577; b) A. Schäfer, C. Huber, R. Ahlrichs, *J. Chem. Phys.* **1994**, *100*, 5829–5835; c) K. Eichkorn, O. Treutler, H. Oehm, M. Häser, R. Ahlrichs, *Chem. Phys. Lett.* **1995**, *242*, 652–660; d) F. Weigend, R. Ahlrichs, *Phys. Chem. Chem. Phys.* **2005**, *7*, 3297–3305; e) F. Weigend, *Phys. Chem. Chem. Phys.* **2006**, *8*, 1057–1065.
[31] P. Deglmann, K. May, F. Furche, R. Ahlrichs, *Chem. Phys. Lett.* **2004**, *384*, 103–107.
[32] a) J. P. Perdew, *Phys. Rev. Lett.* **1996**, *77*, 3865; b) J. P. Perdew, M. Ernzerhof, K. Burke, *J. Chem. Phys.* **1996**, *105*, 9982–9985; c) J. Perdew, K. Burke, M. Ernzerhof, *Phys. Rev. Lett.* **1996**, *77*, 3865-3868, erratum: *Phys. Rev. Lett.* **1997**, *78*, 1396; d) C. Adamo, V. Barone, *J. Chem. Phys.* **1999**, *110*, 6158–

6170; e) M. Ernzerhof, G. E. Scuseria, *J. Chem. Phys.* **1999**, *110*, 5029–5036; f) J. Tao, J. P. Perdew, V. N. Staroverov, G. E. Scuseria, *Phys. Rev. Lett.* **2003**, *91*, 146401; g) J. P. Perdew, J. Tao, V. N. Staroverov, G. E. Scuseria, *J. Chem. Phys.* **2004**, *120*, 6898–6911.

[33] a) S. Grimme, J. Antony, S. Ehrlich, H. Krieg, *J. Chem. Phys.* **2010**, *132*, 154104; b) S. Grimme, S. Ehrlich, L. Goerijk, *J. Comput. Chem.* **2011**, *32*, 1456–1465.

Received: November 8, 2019